



QCD at the Tevatron: Jets and Fragmentation

V. Daniel Elvira^{a *}

^aFermi National Accelerator Laboratory, P.O.Box 500, Batavia, IL 60510

At the Fermilab Tevatron energies, ($\sqrt{s}=1800$ GeV and $\sqrt{s}=630$ GeV), jet production is the dominant process. During the period 1992-1996, the DØ and CDF experiments accumulated almost 100 pb^{-1} of data and performed the most accurate jet production measurements up to this date. These measurements and the NLO-QCD theoretical predictions calculated during the last decade, have improved our understanding of QCD, our knowledge of the proton structure, and pushed the limit to the scale associated with quark compositeness to 2.4-2.7 TeV. In this paper, we present the most recent published and preliminary measurements on jet production and fragmentation by the DØ and CDF collaborations.

1. Introduction

Quantum chromodynamics (QCD) describes the inelastic scattering between a proton and an antiproton as a hard collision between their constituents or partons: quarks or gluons. After the collision, the outgoing partons hadronize into streams of particles called jets. At the Tevatron energies, ($\sqrt{s}=1800$ GeV and $\sqrt{s}=630$ GeV), jet production is the dominant process. During the period 1992-1996, the DØ and CDF experiments accumulated almost 100 pb^{-1} of data and performed the most accurate jet production measurements up to this date. Among the results published in that period and subsequent years, we can cite inclusive jet cross sections, dijet angular distributions, and dijet mass cross sections [1, 2, 3, 4, 5, 6, 7]. At the same time, predictions for jet production rates have improved in the early nineties with next-to-leading order (NLO) perturbative QCD calculations [9] and more accurate parton distribution functions (pdf) [10]. The high center-of-mass energy at the Tevatron and the unprecedented accuracy of the measurements, together with the NLO-QCD theoretical predictions derived during the last decade, have improved our understanding of QCD, our knowledge of the proton structure, and pushed the limit to the scale associated with quark compositeness.

In this paper, we include a summary of some of the most significant jet results published by CDF

and DØ as well as their most recent preliminary measurements. Jet cross sections in forward pseudorapidity regions, cross sections of dijets separated by large pseudorapidity intervals, and sub-jet and particle multiplicity measurements provide information on parton distribution functions, probe BFKL dynamics, explore the jet structure, and study the hadronization process. In the first sections, we describe how jets are selected, reconstructed and calibrated at DØ and CDF. They are followed by sections on each measurement and the conclusion.

2. Jet Reconstruction and Data Selection

For most of the analyses presented here jets are reconstructed using an iterative fixed cone algorithm with a cone radius of $\mathcal{R}=0.7$ in η - ϕ space [12], (pseudorapidity is defined as $\eta = -\ln[\tan(\frac{\theta}{2})]$). This algorithm is applied to calorimeter towers without making use of tracking information, except for the determination of the interaction vertex. The DØ subjet multiplicity measurement uses a K_T algorithm [22, 24, 24] on calorimeter towers, with a resolution parameter $\mathcal{D}=1$ (see Ref. [11].) The CDF particle multiplicity results use fixed cone algorithms with different cone sizes, based on particle information at the tracking level.

The offline data selection procedure eliminates background caused by electrons, photons, noise, or cosmic rays. In the case of DØ it follows the

*Representing the DØ Collaboration

methods described in Refs. [13, 14].

3. Energy Corrections

The jet energy scale correction, described by DØ in Ref. [15], removes instrumentation effects associated with calorimeter response, showering, and noise, as well as the contribution from spectator partons (underlying event).

The DØ energy scale correction corrects the jet E_T from their reconstructed value to their “true” E_T on average (energy of a jet defined from final state hadrons). An unsmearing correction is applied later to remove the effect of a finite E_T resolution [13]. CDF corrects both for scale and resolutions using a Monte Carlo simulation tuned to represent the data.

4. The Inclusive Jet Cross Section at $\sqrt{s} = 1800$ GeV

The inclusive jet cross section is measured by both the DØ (in $|\eta| < 0.5$ and $0.1 < |\eta| < 0.7$) and the CDF experiments (in $0.1 < |\eta| < 0.7$). It is defined as:

$$\frac{d^2\sigma}{dE_T d\eta} = \frac{N_i}{\mathcal{L}_i \epsilon_i \delta E_T \Delta\eta} \quad (1)$$

where N_i is the number of accepted jets in E_T bin i of width ΔE_T , \mathcal{L}_i is the integrated luminosity, ϵ_i is the efficiency of the trigger, vertex selection, and the jet quality cuts, and $\Delta\eta$ is the width of the pseudorapidity bin.

Figure 1 shows the various uncertainties for the DØ ($|\eta| < 0.5$) cross section. The second outermost curve shows the error on the energy scale which varies from 8% at low E_T to 30% at 450 GeV and dominates the total error. Most of the systematic uncertainties of the inclusive jet cross section are highly correlated as a function of E_T .

Figure 2 show the fractional difference between the data, D , and a JETRAD theoretical prediction, T , normalized by the prediction, $((D-T)/T)$, for $|\eta| < 0.5$. The JETRAD prediction was generated with $\mu = 0.5E_{Tmax}$, $\mathcal{R}_{sep} = 1.3$ and several different choices of pdf. The error bars represent statistical errors only. The outer bands represent the total cross section error excluding the 5.0%

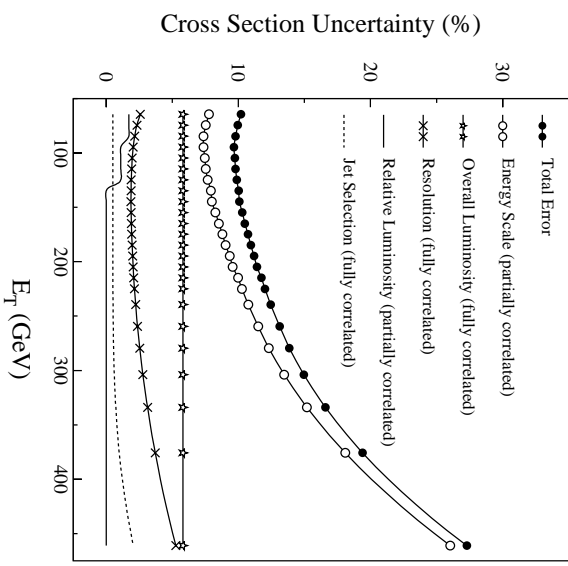


Figure 1. Contributions to the DØ jet ($|\eta| \leq 0.5$) cross section uncertainty plotted by component.

luminosity uncertainty. Given the experimental and theoretical uncertainties, the predictions are in agreement with the data; in particular, the data above $E_T = 350$ GeV show no indication of an excess relative to QCD.

The data and theory can be compared quantitatively with a χ^2 test incorporating the uncertainty covariance matrix. The χ^2 is given by:

$$\chi^2 = \sum_{i,j} \delta_i V_{ij}^{-1} \delta_j \quad (2)$$

where δ_i is the difference between the data and theory for a given E_T bin, and V_{ij} is element i, j of the covariance matrix:

$$V_{ij} = \rho_{ij} \cdot \Delta\sigma_i \cdot \Delta\sigma_j. \quad (3)$$

where $\Delta\sigma$ is the sum of the systematic error and the statistical error added in quadrature if $i = j$ and the systematic error if $i \neq j$, and ρ_{ij} is the correlation between the systematic uncertainties of E_T bins.

All but one of the JETRAD predictions adequately describe the $|\eta| \leq 0.5$ and $0.1 \leq |\eta| \leq 0.7$ (shown in Figure 3) cross sections (probabilities for χ^2 to exceed the calculated value are between 10% and 86%). The prediction using CTQ4HJ

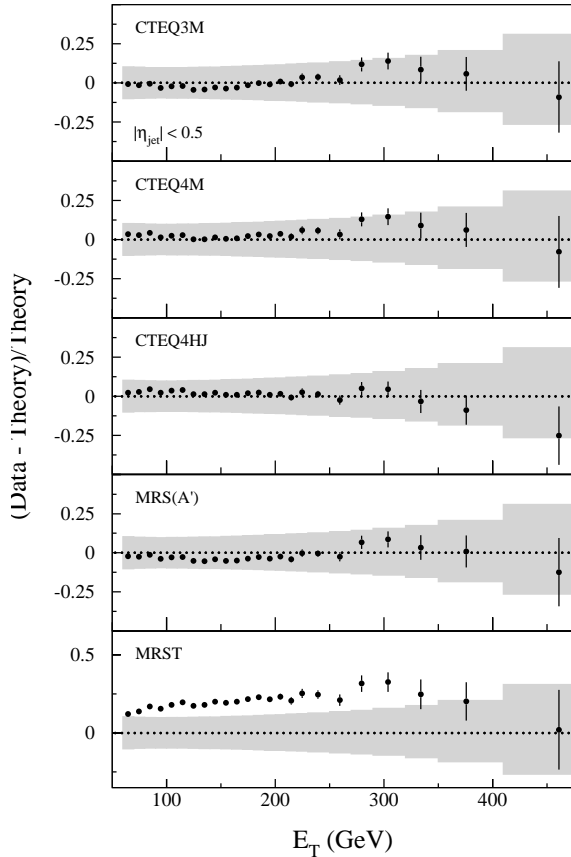


Figure 2. The difference between $D\bar{O}$ data and JETRAD QCD predictions normalized to predictions for $|\eta| < 0.5$. The shaded region represents the $\pm 1\sigma$ systematic uncertainties about the prediction.

and $\mu = 0.5E$ produces the highest probability for both measurements. The prediction with the MRSTGD pdf has a probability of agreement with the data of 0.3%, and is incompatible with the data.

The top panel in Fig. 3 shows $(D - T)/T$ for the $D\bar{O}$ data in the $0.1 \leq |\eta| \leq 0.7$ region relative to a JETRAD calculation using the CTEQ4HJ pdf, $\mu = 0.5E_{Tmax}$, and $\mathcal{R}_{sep} = 2.0\mathcal{R}$. Also included is the published CDF measurement from the 1992-93 Tevatron running period [2] relative to the same JETRAD prediction. The CDF measurement shows an excess with respect to the theory at high E_T , which can be accommodated by adjusting the gluon pdf (CTEQ4HJ set). If we include the systematic uncertainties of the two

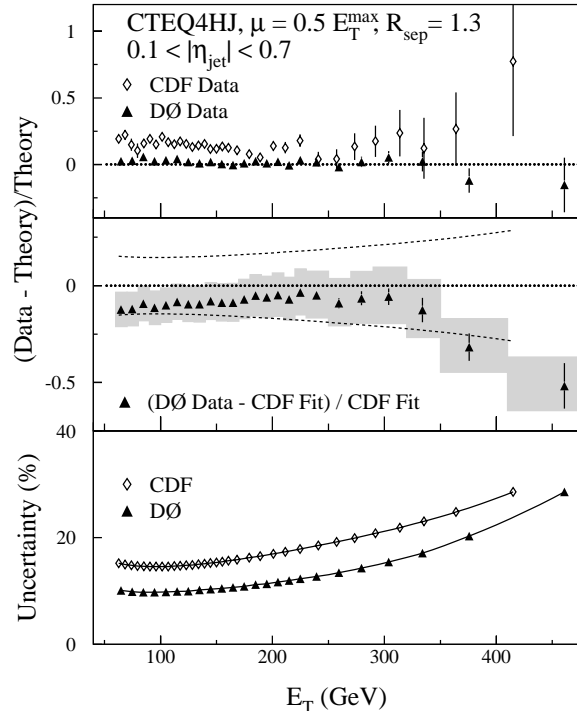


Figure 3. Top: Normalized comparisons of the $D\bar{O}$ data and of the CDF data to a JETRAD prediction (CTEQ4HJ and $\mu = 0.5E_{Tmax}$). Middle: Difference between the data and smoothed results of CDF normalized to the latter. The shaded region represents the $\pm 1\sigma$ systematic uncertainties about the $D\bar{O}$ data. The dashed curves show the $\pm 1\sigma$ systematic uncertainties about the smoothed CDF data. Bottom: A comparison of the systematic uncertainties of both experiments.

experiments (CDF's uncertainties in Ref. [2]) in a covariance matrix, the χ^2 is 30.8 for 24 degrees of freedom (probability of 16%), representing acceptable agreement between $D\bar{O}$ and CDF.

5. Inclusive Jet Cross Section at $\sqrt{s} = 630$ GeV

Figure 4 shows the fractional difference between the $D\bar{O}$ data and several JETRAD predictions given different choices of renormalization scale and pdf. These NLO QCD predictions are in reasonable agreement with the data. The data and predictions are compared quantitatively with

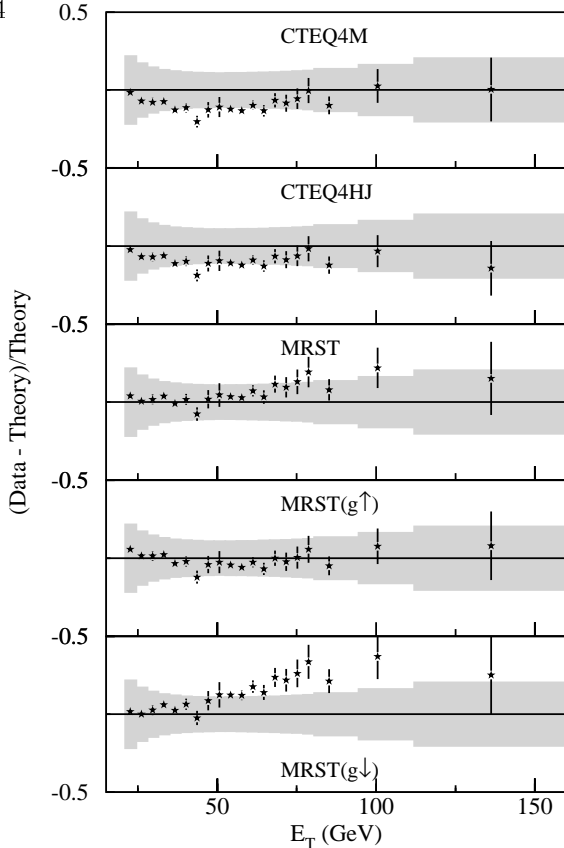


Figure 4. $(D-T)/T$ for the DØ 630 GeV jet cross section. $(|\eta_{jet}| < 0.5)$. The solid stars represent the data compared to the calculation for $\mu = 0.5E_{Tmax}$ and the pdfs CTEQ4M , CTEQ4HJ , MRST , MRSTGU and MRSTGD . The shaded region represents the $\pm 1\sigma$ systematic uncertainty. a χ^2 test. All but two of the JETRAD predictions adequately describe the cross section at $\sqrt{s} = 630$ GeV (the probabilities for χ^2 to exceed the calculated values are between 10% and 74%). The prediction using MRSTGU and $\mu = 0.5E_{Tmax}$ produces the highest probability. The prediction with MRSTGD pdf and $\mu = 0.5E_{Tmax}$, and CTEQ3M pdf and $\mu = 2E_{Tmax}$ are ruled out by the DØ measurement (agreement probability $\leq 0.4\%$).

6. The Ratio of Jet Cross Sections

The dimensionless inclusive jet cross section is given by

$$\sigma_{CM} = \frac{E_T^3}{2\pi} \frac{d^2\sigma}{dE_T d\eta}, \quad (4)$$

where $d^2\sigma/dE_T d\eta$ is given by Eq. 1, and x is the center-of-mass energy. A naive parton model with no Q^2 dependence of the pdfs, and therefore no running of α_s , predicts this cross section ratio to be unity, that is independent of the center-of-mass energy of the $\bar{p}p$ system. The observable is nearly insensitive to the choice of parton distribution functions. It is, therefore, a more stringent test of QCD matrix elements.

DØ has measured the ratio of inclusive jet cross sections in the central pseudorapidity bin $(|\eta| < 0.5)$ [8]. This quantity is calculated in bins of identical x_T :

$$R(x_T) = \frac{\sigma_{630}(x_T)}{\sigma_{1800}(x_T)}. \quad (5)$$

The inclusive jet cross section errors are highly correlated as a function of E_T and center-of-mass energy and will cancel in the ratio. The energy scale uncertainty dominates the total error in the ratio too.

Figure 5 shows the ratios of cross sections with JETRAD predictions using different pdfs. The measured ratios lie approximately 10% below the theoretical predictions, which have an uncertainty of about 10%. The χ^2 values lie in the range 15.1-24 for 20 degrees of freedom (corresponding to probabilities in the range 28% to 77%). The best agreement occurs for extreme choices of renormalization scales ($\mu = 0.25, 2E_{Tmax}$).

In general, the NLO-QCD predictions yield satisfactory agreement with the DØ data for standard choices of renormalization scale or pdfs. In terms of the normalization, however, the absolute values of the standard predictions lie consistently and significantly higher than the data.

CDF has also measured the ratio of central jet cross sections. Figure 6 shows a preliminary result by CDF compared with NLO-QCD predictions (and the DØ measurement). Although the data and the theory agree in shape at high x_T , there is a significant deviation at low values.

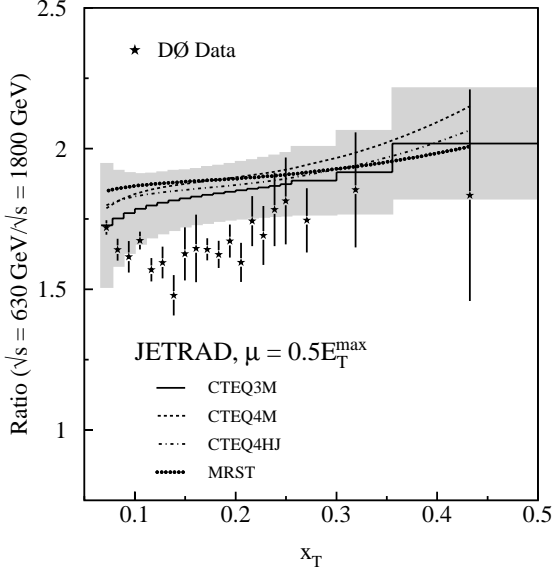


Figure 5. The DØ ratio of dimensionless cross sections compared with JETRAD predictions ($\mu = 0.5E_{Tmax}$ and the CTEQ3M , CTEQ4M , CTEQ4HJ , or MRST pdfs). The shaded band represents the $\pm 1\sigma$ systematic uncertainty.

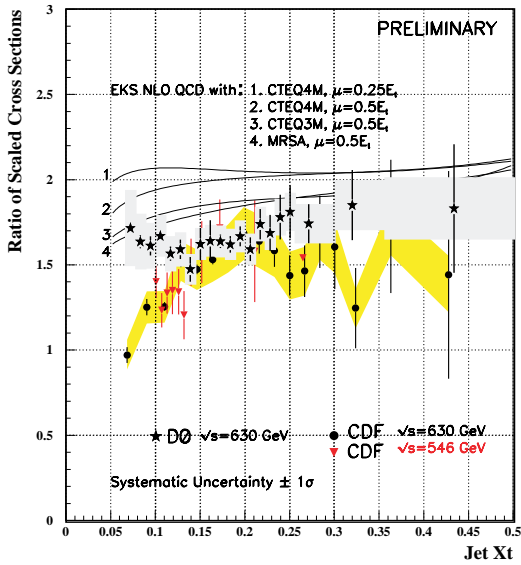


Figure 6. The DØ and CDF ratio of dimensionless cross sections compared with each other and the JETRAD predictions.

7. The Forward Jet Cross Sections at $\sqrt{s} = 1800$ GeV

DØ has performed preliminary measurements of forward jet cross sections up to pseudorapidities of $|\eta| = 3$. These measurements allow to reach regions in (x, Q^2) space previously unexplored. Figure 7 shows a comparison of the measured cross sections in five different η bins with the JETRAD prediction (CTEQ4HJ or MRST, and $\mu = E_{Tmax}/2$). Within the experimental and theoretical uncertainties, the measurement and the calculation are in good agreement. χ^2 studies are underway for a quantitative statement.

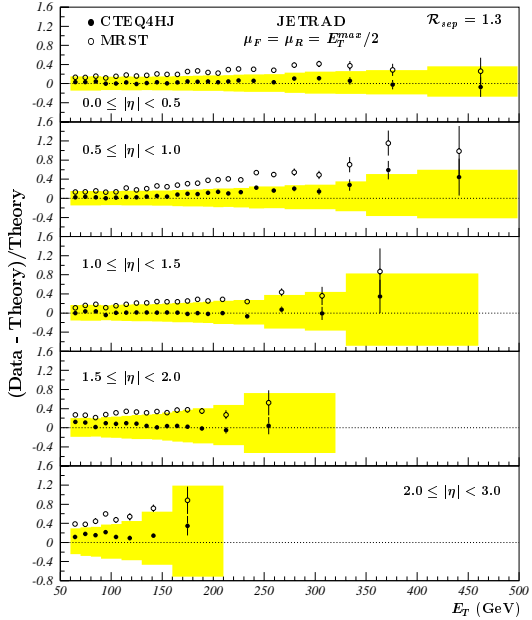


Figure 7. Pseudorapidity dependence of the inclusive jet cross section ($|\eta| < 3$), compared with NLO QCD (CTEQ4HJ: full circles, MRST: open circles). The bands represent the total systematic uncertainties in the experiment.

8. The Ratio of Dijet Mass Spectra at $\sqrt{s} = 1800$ GeV

The dijet mass spectrum is calculated using the relation:

$$\kappa \equiv \frac{d^3\sigma}{dM_{JJ}d\eta_1d\eta_2} = \frac{N_i}{\mathcal{L}_i\epsilon_i\Delta M_{JJ}\Delta\eta_1\Delta\eta_2}, \quad (6)$$

where N_i is the number of events in mass bin i ; \mathcal{L}_i is the integrated luminosity; ϵ_i is the efficiency of the trigger, vertex selection, and the jet quality cuts; ΔM_{JJ} is the width of the mass bin; and $\Delta\eta_{1,2}$ are the widths of the pseudorapidity bin. At DØ the cross section is measured for the pseudorapidity bin $|\eta_{jet}| < 1.0$. The systematic errors are dominated by the uncertainties due to the jet energy scale, which are 7% (30%) for the 209 (873) GeV mass bins.

The dijet mass cross section measurement was then repeated for $|\eta_{jet}| < 0.5$, and $0.5 < |\eta_{jet}| < 1.0$ and their ratio was determined. A large fraction of the total error cancels, as well as the uncertainty in the theoretical prediction of the ratio which is less than 3% due to the choice of pdf, and 6% from the choice of renormalization and factorization scale (excluding $\mu = 0.25E_{Tmax}$). By taking the ratio $\kappa(|\eta_{jet}| < 0.5) / \kappa(0.5 < |\eta_{jet}| < 1.0)$ the systematic uncertainties decrease to less than 10%.

Given the experimental and theoretical uncertainties, the prediction can be regarded as in good agreement with the data (see Fig. 8). The data are also in agreement, within the uncertainties, with the cross section measured by CDF [6].

All choices of pdfs and renormalization scales are in good agreement with the data (χ^2) test, except for $\mu = 0.25E_{Tmax}$ which is excluded by the data.

The ratio of the mass spectra is used to place limits on quark compositeness. The PYTHIA event generator is used to simulate the effect of compositeness by taking the ratio of these LO predictions with compositeness, to the LO with no compositeness, and scaling with this factor the JETRAD NLO prediction (shown in Fig. 8).

The DØ data shows no evidence of compositeness. The dijet mass spectrum rules out quark compositeness models at the 95% confidence level

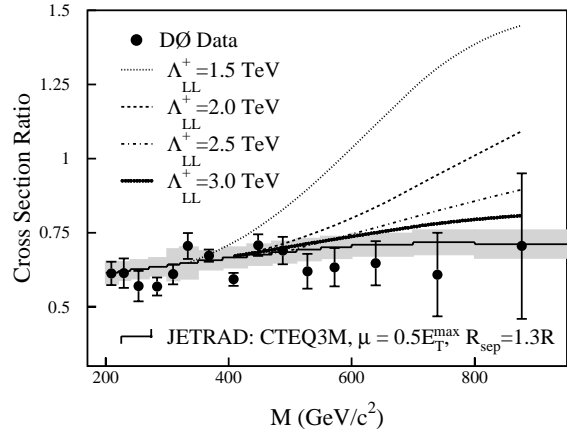


Figure 8. The ratio of dijet mass cross sections for $|\eta_{jet}| < 0.5$ and $0.5 < |\eta_{jet}| < 1.0$ for data (solid circles) and theoretical predictions for compositeness models with various values of Λ_{LL}^+ . The error bars show the statistical uncertainties. The shaded region represents the $\pm 1\sigma$ systematic uncertainty.

where Λ_{LL}^+ is below 2.7 TeV and Λ_{LL}^- is below 2.4 TeV.

9. The Triple Differential Jet Cross Sections at $\sqrt{s} = 1800$ GeV

Both CDF and DØ have performed preliminary measurements of triple differential jet cross sections. This observable is defined only in terms of the two leading jets of the event, to provide information on pdfs. In particular, the Tevatron probes high Q^2 and x values previously unreachable.

CDF defines the triple differential jet cross section as $\frac{d^3\sigma}{dE_{T1}d\eta_1d\eta_2}$, where E_{T1} is the transverse energy of a central jet in the event, and η_1, η_2 are the pseudorapidities of the central and forward jets, respectively. This quantity is measured as a function of the transverse energy of the central jet for different η_2 bins up to $|\eta|=3$.

DØ measures $\frac{d^3\sigma}{dE_Td\eta_1d\eta_2}$ versus E_T , where E_T is the transverse energy of the central or the forward jet (the event enters twice in the measurement). This quantity is measured for different η_2 bins up to $|\eta|=2$. The main difference between the CDF and DØ observables is that DØ measures the E_T of both jets and CDF measures only the E_T of the central jet.

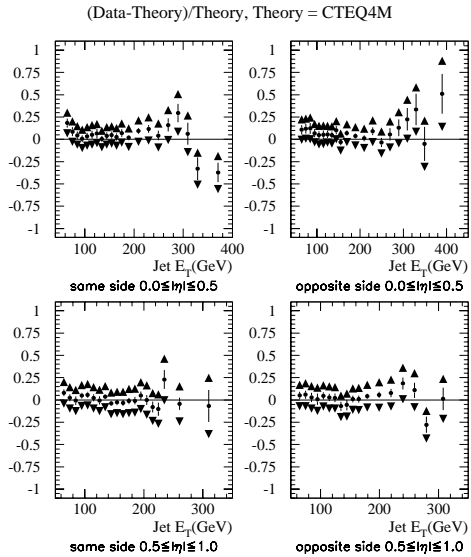


Figure 9. $D\bar{O}$ triple differential jet cross sections in different $|\eta_2| < 2$ intervals for the two leading jets (central and forward) in the same pseudorapidity side (sign of η_1 same as sign of η_2).

Figures 9- 10 show the $D\bar{O}$ measurement in different η_2 bins for the two leading jets (central and forward) in the same pseudorapidity side (sign of η_1 same as sign of η_2), and opposite sides. Each configuration is adequate for learning about different pdfs in different regions of (x, Q^2) space. For example, two forward jets in the same side are associated with one incoming parton with high x and the other with low x . Figure 11 shows the CDF result for different η_2 bins, independently of the relative sign of η_1 and η_2 .

Qualitatively, there is good agreement between data and theory. Both experiments are currently working on quantitative studies.

10. Dijet Cross Sections at Large η Intervals

At high center-of-mass energies, \sqrt{s} , and for momentum transfers, Q , fixed and $\ll \sqrt{s}$, the radiative corrections to the parton-parton scattering contain large logarithms $\ln(s/Q^2)$, which need to be summed to all orders in α_s . This summation is accomplished by the Balitsky-Fadin-Kuraev-Lipatov (BFKL) equation [16].

Inclusive dijet production provides an ideal possible signature of BFKL dynamics. For large

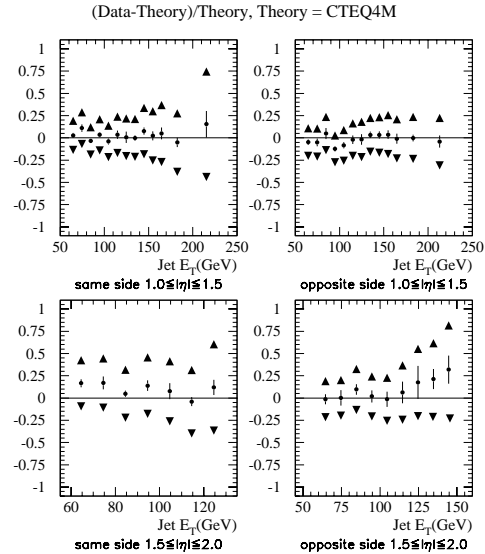


Figure 10. $D\bar{O}$ triple differential jet cross sections in different $|\eta_2| < 2$ intervals for the two leading jets (central and forward) in opposite pseudorapidity sides (sign of η_1 opposite of sign of η_2).

values of the jet longitudinal momentum fraction, x_j , the large logarithms $\ln(s/Q^2)$ result in large $\ln(\hat{s}/Q^2)$ (where $\sqrt{\hat{s}}$ is the partonic center-of-mass energy) which factorize in the partonic dijet cross section, $\hat{\sigma}$. The $\ln(\hat{s}/Q^2)$ terms are of the order of the pseudorapidity interval, $\Delta\eta$, between the two jets [17] ($\eta = -\ln(\tan(\theta/2))$, where θ is the polar angle of the jet relative to the proton beam).

$D\bar{O}$ performed a measurement of the dijet cross section at two different center-of-mass energies, $\sqrt{s_A} = 1800$ GeV and $\sqrt{s_B} = 630$ GeV, using the $D\bar{O}$ detector at the Fermilab Tevatron. The kinematics of the event is reconstructed using the most forward/backward jets, and the cross section is measured as a function of x_1 , x_2 and Q^2 at each center-of-mass energy. The ratio of the cross sections is then determined at the same values of x_1 , x_2 and Q^2 between the two energies. This eliminates the dependence of the cross section on the pdf's and reduces the ratio to that of the partonic cross sections. It can be shown [7] that the latter is a function only of the pseudorapidity separations between the two jets ($\Delta\eta$'s):

$$R = \frac{\hat{\sigma}(\Delta\eta_A)}{\hat{\sigma}(\Delta\eta_B)} = \frac{e^{(\alpha_{BFKL}-1)(\Delta\eta_A-\Delta\eta_B)}}{\sqrt{\Delta\eta_A/\Delta\eta_B}}. \quad (7)$$

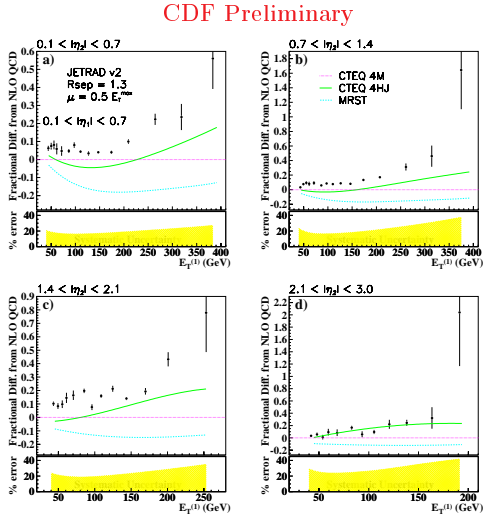


Figure 11. CDF triple differential jet cross sections for different η_2 bins.

In other words, variation of \sqrt{s} , while keeping x_1 , x_2 and Q^2 fixed, is equivalent to variation of $\Delta\eta$, which directly probes the BFKL dynamics.

Several theoretical predictions can be compared to the $D\bar{O}$ measurement. Leading Order QCD predicts the ratio of the cross sections to fall asymptotically toward unity. The HERWIG [19] Monte Carlo provides a more realistic prediction. It calculates the exact $2 \rightarrow 2$ subprocess including initial and final state radiation and angular ordering of the emitted partons. The LLA BFKL intercept for $\alpha_s(20 \text{ GeV}) = 0.17$ [18] is equal to 1.45. The Next-to-Leading Logarithmic [20] are not as yet available.

The ratio of cross sections is shown in Fig. 12 as a function of the mean pseudorapidity interval at 630 GeV. It is evident that the growth of the dijet cross section with $\Delta\eta$ is stronger in the data than in any theoretical model which was considered. Namely, the measured ratio is higher by 4 standard deviations than the LO prediction, 3 deviations than the HERWIG prediction, and 2.3 deviations than the LLA BFKL one.

11. Subject Multiplicities

A jet is typically associated with the energy and momentum of each final state parton. Experimentally, however, it is a cluster of energy in the calorimeter. QCD predicts that gluons radiate more than quarks. Asymptotically, the ratio

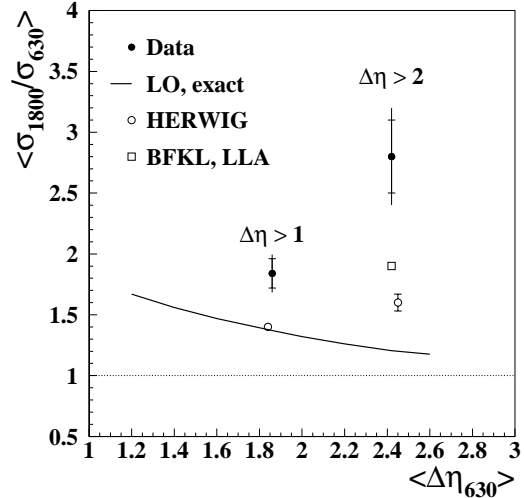


Figure 12. The $D\bar{O}$ ratio of the dijet cross sections at both center-of-mass energies for $\Delta\eta > 1$ and $\Delta\eta > 2$. The inner error bars on the data points represent statistical uncertainties; the outer bars represent statistical and uncorrelated systematic uncertainties added in quadrature. The error bars on the HERWIG predictions represent statistical uncertainties.

of objects within gluon jets to quark jets is expected to be in the ratio of their color charges $C_A/C_F = 9/4$ [21].

$D\bar{O}$ performed a preliminary measurement of subjet multiplicities in quark and gluon jets, as well as the ratio of the means of these two quantities. For this analysis, jets are reconstructed using the K_T algorithm [22, 23, 24] with a resolution parameter $\mathcal{D}=1$ (see Ref. [11]).

M is the subjet multiplicity in a mixed sample of quark and gluon jets. It may be written as a linear combination of subjet multiplicity in gluon and quark jets:

$$M = fM_g + (1 - f)M_q \quad (8)$$

The coefficients are the fractions of gluon and quark jets in the sample, f and $(1 - f)$, respectively. Consider Eq. (8) for two samples of jets in the same kinematic range, one at $\sqrt{s} = 1800$ (gluon dominated) and the other at 630 GeV (quark dominated), assuming M_g and M_q are independent of \sqrt{s} . The solutions are

$$M_q = \frac{f^{1800}M^{630} - f^{630}M^{1800}}{f^{1800} - f^{630}} \quad (9)$$

$$M_g = \frac{(1 - f^{630}) M^{1800} - (1 - f^{1800}) M^{630}}{f^{1800} - f^{630}} \quad (10)$$

where M^{1800} and M^{630} are the experimental measurements in the mixed jet samples at $\sqrt{s} = 1800$ and 630 GeV, and f^{1800} and f^{630} are the gluon jet fractions in the two samples. The method relies on knowledge of the two gluon jet fractions.

Figure 13 shows that the subjet multiplicity is clearly larger for gluon jets compared to quark jets. The gluon jet fractions are the largest source of systematic error. The measured ratio and its total uncertainty are: $R = \frac{\langle M_g \rangle - 1}{\langle M_q \rangle - 1} = 1.91 \pm 0.04(\text{stat})_{-0.19}^{+0.23}(\text{sys})$. The ratio is well described by the HERWIG parton shower Monte Carlo, and is only slightly smaller than the naive QCD prediction $9/4$.

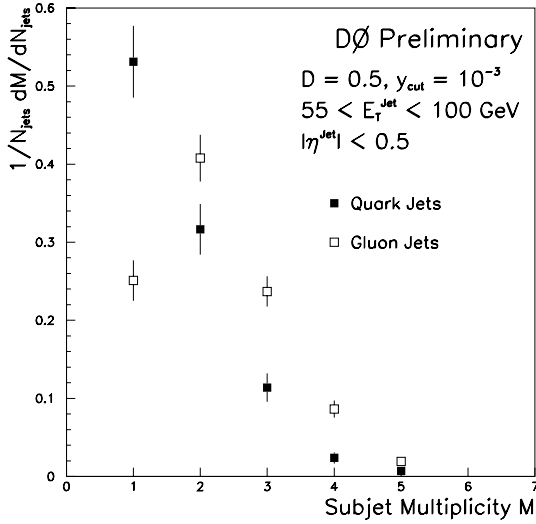


Figure 13. Corrected subjet multiplicity in quark and gluon jets, extracted from DØ data.

12. Particle Multiplicities

Perturbative QCD calculations, carried out in the framework of the Modified Leading Log Approximation [25] (MLLA), complemented with the Local Parton-Hadron Duality Hypothesis [26] (LPHD), predict the shape of the momentum distribution, as well as the total inclusive multiplicity, of particles in jets. The MLLA is an asymptotic calculation, which proves to be infrared sta-

ble, in the sense that the model cutoff parameter Q_{eff} can be safely pushed down to Λ_{QCD} . LPHD is responsible for the hadronization stage and implies that hadronization is local and happens at the end of the parton shower development. In its simplest interpretation, the model has one parameter K_{LPHD} , the rate of parton-to-hadron conversion:

$$N_{hadrons} = K_{LPHD} \times N_{partons}. \quad (11)$$

In MLLA, momentum distributions and multiplicities in quark and gluon jets in a restricted cone of size θ around the jet axis are functions of $E_{jet}\theta/Q_{eff}$ [27] and differ by a factor r :

$$N^{q-jet}(\xi) = \frac{1}{r} N^{g-jet}(\xi)$$

$$\xi = \log \frac{1}{x}, x = p_{track}/E_{jet} \quad (12)$$

Jets at the Tevatron are a mixture of quark and gluon jets. Therefore,

$$N_{hadrons}^{charged}(\xi) =$$

$$K_{LPHD}^{charged}(\epsilon_g + (1 - \epsilon_g)\frac{1}{r}) F^{nMLLA} N_{part}^{q-jet}(\xi) =$$

$$K N_{part}^{q-jet}(\xi) \quad (13)$$

where ϵ_g is the fraction of gluon jets in the events, the factor of $1/r$ reflects the difference between gluon and quark jets, and, finally, the factor F^{nMLLA} accounts for the next-to MLLA corrections to the gluon spectrum. Theoretical calculations [28] predict somewhat different values of F^{nMLLA} , but all agree that F^{nMLLA} has almost no dependence on the jet energy in the region relevant to this analysis. The average of the results above was chosen and the difference between predictions was used as a theoretical error: $F^{nMLLA} = 1.3 \pm 0.2$. The same papers predict the value of r to be between 1.5 and 1.8.

12.1. The Dijet Data Analysis

CDF data collected during the 1993-1995 running period was used for this analysis. Events with two jets well balanced in transverse energy were selected. Both jets were required to be in the

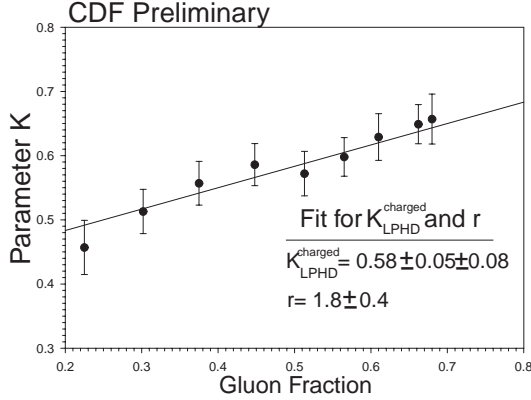


Figure 14. Fit of the parameter K for K_{LPHD} and r . Cone 0.47. First error is combined statistical and systematic errors, the second one - theoretical error coming from F^{nMLLA} .

central region. Tracks were counted in restricted cones of sizes 0.28, 0.36 and 0.47 around the jet axis.

Analysis of the fitted parameter K allows an extraction of both K_{LPHD} and r . According to Eq. 13, the dependence is linear. Figure 14, shows 9 values of K (corresponding to 9 dijet masses for the largest cone-size 0.47) vs the gluon jet fraction (extracted using Herwig 5.6) in the events from respective dijet mass bins, as well as the results of the fit for K_{LPHD} and r . The same parameters can be extracted from the inclusive multiplicity using an integrated version of Eq. 13. In this case, the extracted parameters will only rely on the total multiplicity and not on the exact shape of the distribution. Figure 15 shows the fit of data with MLLA predictions as well as the fitted parameters K_{LPHD} and r . It is remarkable that the two results are in such a good agreement.

12.2. Model-Independent Measurement

The multiplicity in dijet and γ -jet events is compared (data selection was similar) to extract model-independent measurement of r . These samples have very different fraction of gluon jets for the jet energies 40-60 GeV (roughly 60% for dijets and 12% for γ -jet, according to Herwig 5.6). The multiplicities measured for each of the samples and a knowledge of the gluon jet fractions

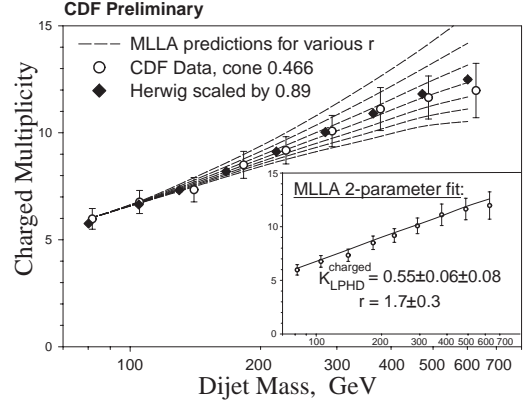


Figure 15. Charged particle multiplicity (per jet) as a function of the dijet mass. MLLA fit for K_{LPHD} and r .

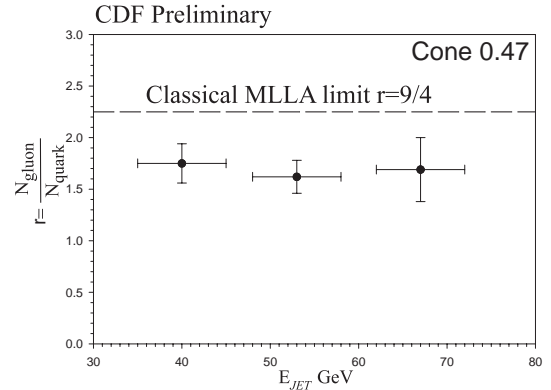


Figure 16. Ratio of charged multiplicities in gluon and quark jets based on comparison of the dijet and γ -jet events.

allowed to extract r . Figure 16 shows the measured r as a function of the jet energy. The result for r is $1.75 \pm 0.11 \pm 0.15$ in perfect agreement with MLLA result.

13. Conclusions

The 1992-1996 collider run at Fermilab represented a major step in the testing of QCD. The DØ and CDF experiments measured jet cross sections with unprecedented accuracy, extended the energy reach to ~ 450 GeV, and set a new limit of 2.4-2.7 TeV for the quark compositeness scale. In general, and within experimental and theoretical uncertainties, QCD is in good agreement with

the data. Measurements on jet structure and fragmentation were also performed and yielded agreement with QCD; they support the perturbative nature of jet fragmentation. The upcoming run at the Tevatron, scheduled to start in March 2001, will extend the energy frontier even further ($\sqrt{s}=2$ TeV) and collect at least 20 times more data, allowing precision measurements of QCD in kinematic regions previously unexplored.

REFERENCES

1. B. Abbott *et al.* (DØ Collaboration), Phys. Rev. Lett. **82**, 2451-2456 (1999).
2. F. Abe *et al.* (CDF Collaboration), Phys. Rev. Lett. **77**, 438 (1996).
3. B. Abbott *et al.* (DØ Collaboration), Phys. Rev. Lett. **80**, 666-671 (1997).
4. F. Abe *et al.* (CDF Collaboration), Phys. Rev. Lett. **77**, 5336-5341 (1996).
5. B. Abbott *et al.* (DØ Collaboration), Phys. Rev. Lett. **82**, 2457-2462 (1999).
6. T. Affolder *et al.* (CDF Collaboration). Submitted to Phys. Rev. D (1999).
7. B. Abbott *et al.* (DØ Collaboration), Phys. Rev. Lett. **84**, 5722 (2000).
8. B. Abbott *et al.* (DØ Collaboration), Submitted to Phys. Rev. Lett.
9. W. T. Giele, E. W. N. Glover, and D. A. Kosower, Phys. Rev. Letters **73**, 2019 (1994); S. D. Ellis, Z. Kunszt, and D. E. Soper, Phys. Rev. Letters **64**, 2121 (1990); F. Aversa *et al.*, Phys. Rev. Letters **65**, (1990)
10. H. L. Lai *et al.*, Phys. Rev. D **51**, 4763 (1995); A. D. Martin *et al.*, Eur. Phys. J.C **4**, 463-496 (1998).
11. R. Snihur (DØ Collaboration), 7th International Workshop on Deep Inelastic Scattering and QCD DESY Zeuthen, Germany 19-23 Apr 1999. Nuclear Physics B (Proc. Suppl.) **79**, 494-496 (1999).
12. B. Abbott *et al.*, Eur. Phys. J. C. **5**, 687 (1998).
13. L. Babukhadia, Ph.D. Thesis, University of Arizona, 1999 (unpublished), [HTTP://WWW-D0.FNAL.GOV/RESULTS/PUBLICATIONS_TALKS/THESIS/THESIS.HTML](http://www-d0.fnal.gov/results/publications_talks/thesis/thesis.html).
14. J. Krane, Ph.D. Thesis, University of Nebraska-Lincoln, 1998 (unpublished), [HTTP://WWW-D0.FNAL.GOV/RESULTS/PUBLICATIONS_TALKS/THESIS/THESIS.HTML](http://www-d0.fnal.gov/results/publications_talks/thesis/thesis.html).
15. B. Abbott *et al.*, (DØ Collaboration), Nuc. Inst. and Meth. A **424**, nos. 2-3, 352-394 (1999)
16. L.N. Lipatov, Sov. J. Nucl. Phys. **23**, 338 (1976); E.A. Kuraev, L.N. Lipatov, and V.S. Fadin, Sov. Phys. JETP **44** (1976) 443; Sov. Phys. JETP **45**, 199 (1977); Y.Y. Balitsky and L.N. Lipatov, Sov. J. Nucl. Phys. **28**, 822 (1978).
17. A.H. Mueller and H. Navelet, Nucl. Phys. **B282** 727 (1987).
18. L.H. Orr and W.J. Stirling, Phys. Lett. B **429** 135 (1998).
19. G. Marchesini *et al.*, Comp. Phys. Comm. **67** 465 (1992).
20. V.S. Fadin and L.N. Lipatov, Phys. Lett. B **429**, 127 (1998); G. Camici and M. Ciafaloni, Phys. Lett. B **430**, 349 (1998).
21. R.K. Ellis, W.J. Stirling, and B.R. Webber, QCD and Collider Physics, Cambridge University Press, 1996.
22. S.D. Ellis and D.E. Soper, Phys. Rev. D **48** (1993) 3160.
23. S. Catani, Yu.L. Dokshitzer, and B.R. Webber, Phys. Lett. B **285** (1992) 291.
24. S. Catani, Yu.L. Dokshitzer, M.H. Seymour, B.R. Webber, Nucl. Phys. B **406** (1993) 187.
25. Yu. Dokshitzer, S. Troyan, *XIX Winter School of LNPI*, vol. 1, p. 144 (1984); A. H. Mueller, *Nucl. Phys. B* **213**, 85 (1983).
26. Ya. I. Azimov, Yu. Dokshitzer, V. Khoze, and S. Troyan, *Z. Phys. C* **27**, 65 (1985).
27. V. A. Khoze and W. Ochs, *Int. J. Mod. Phys. A* **12**, 2949-3120 (1997).
28. S. Catani *et al.*, *Nucl. Phys. B* **377**, 445 (1992); S. Lupia, W. Ochs, Nucl. Phys. (Proc. Suppl.) **64**, 74 (1998).